Correlated percolation and disordered Ising magnetism in doped double perovskites

Tanmay Paramekanti[1]

[1] *Bur Oak Secondary School, 933 Bur Oak Ave, Markham, Ontario, Canada L6E 1G4*

(Dated: November 19, 2024)

Double perovskites are compounds with chemical formula $A_2BB'O_6$ where B and B' ions each form face-centered cubic (fcc) lattices. Recent experiments have studied doped double perovskite $Ba_2Na_{1-x}Ca_xOsO_6$ where $0 \leq x \leq 1$. For $x = 1$, the octupolar magnetism of osmium Os^{6+} on the fcc lattice is well described by an Ising model. To understand this system for dopings $x < 1$, we construct a model where, starting from $x = 1$, each doped Na^+ on a random B site totally suppresses the osmium Ising magnetism on its six neighboring B' sites. This leads to a *correlated* percolation problem on the fcc lattice of osmium ions. Using Monte Carlo simulations, we compute the percolation threshold $x_c \approx 0.7255$ below which osmium Os^{6+} magnetism does not percolate. Based on system sizes we have studied, the fractal dimension of the critical spanning cluster in this correlated percolation model is found to be $d_f \approx 2.37$. We also use Monte Carlo simulations to compute the configuration averaged specific heat and transition temperature T_c of the Ising model on the largest cluster for $x > x_c$, and compare our results on T_c versus doping with experiments.

I. INTRODUCTION

Double perovskite materials, with the general formula $A_2BB'O_6$, are of great interest due to the possibility of substituting ions at the A, B, and B' sites in order to realize a large class compounds exhibiting a wide range of magnetic and optical properties [1–10]. Oxide-based and halide-based double perovskites have been proposed for spintronic technologies as well as for photovoltaic applications [11, 12]. Due to a wide range of achievable d-orbital electron fillings, and the interplay of spin-orbit coupling and lattice deformations for heavy elements [13, 14], double perovskite materials also provide unusual examples of d-orbital multipolar magnetism. Quadrupolar magnetism has been reported in the d^1 double perovskites where it is accompanied by lattice distortions [15–24] while Ising type octupolar magnetism has been proposed to explain the observed time-reversal breaking without any dipole moment observed in d^2 double perovskites with osmium Os^{6+} on the fcc lattice [25–33].

Recent experiments and theories have explored the doped double perovskites $Ba_2Na_{1-x}Ca_xOsO_6$ [22, 34]. Substituting a Ca^{2+} ion with Na^+ ions results in six neighboring Os^{6+} ions transitioning to $Os^{6+\varepsilon}$. Each Na^+ dopant also leads to a strong local strain field which completely suppresses the Ising octupolar magnetism on the six neighboring osmium sites [33]. In this paper, we use Monte Carlo simulations to explore the unusual percolation model which arises from the correlated impact of dopants on the osmium octupoles, and study the octupolar Ising model on the percolation cluster. The main results we obtain are: (i) the percolation threshold $x_c \approx 0.7255(10)$ (i.e., Na^+ doping $0.2745(10)$) for the correlated percolation model on the fcc lattice, (ii) the fractal dimension of the percolation cluster $d_f \approx 2.37$ based on system sizes we have studied, and (iii) the doping dependence of the specific heat for the percolating cluster, and the octupolar transition temperature T_c which we compare with muon spin rotation (μSR) data [22].

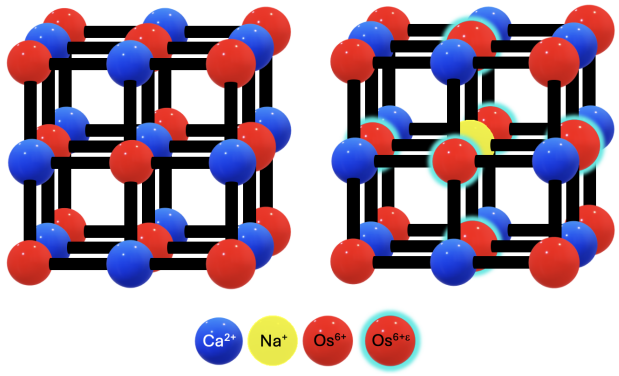

FIG. 1. Left: Ordered double perovskite structure of Ba_2CaOsO_6 consisting of a three-dimensional checkerboard pattern of OsO_6 (red) and CaO_6 (blue) octahedra with the osmium ions exhibiting Ising octupolar magnetism. Ba and oxygen ions are not explicitly depicted. Right: Replacing Ca^{2+} (blue) by Na^+ dopant (yellow) leads to local charge doping as well as strong local strain fields which completely suppress the octupole moment on the six highlighted neighboring osmium sites defining a correlated percolation problem. A nonzero octupolar T_c is only present for sufficiently small Na^+ concentration $(1-x)$ which can support the percolation of Ising magnetic octupoles on the active osmium sites.

II. CORRELATED PERCOLATION MODEL

We define the correlated percolation model as follows. We start at $x = 1$ with the ideal cubic lattice having a checkerboard pattern of Ca^{2+} and Os^{6+} ions as depicted in Fig. 1(a). We assume periodic boundary conditions (PBCs), and define the linear dimension of the system as L, so there are $L^3/2$ ions of each type. At $x = 1$, this structure has the Os^{6+} ions forming an ideal fcc lattice and it exhibits Ising octupolar magnetic order. We next assume that each Ca^{2+} ion, when substituted by Na^+, suppresses the octupolar magnetism on its six neighboring osmium sites as depicted by the highlighted sites in

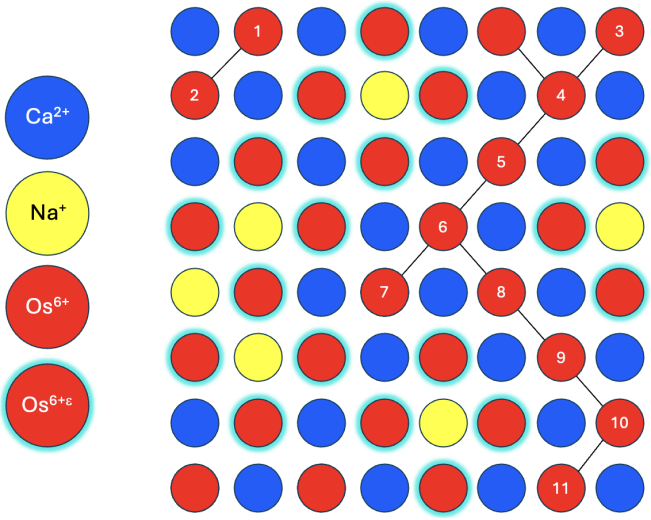

FIG. 2. Depth first search (DFS) traversal order in a 2D slice through the fcc lattice, where we start from an arbitrary Os^{6+} site on one face of the lattice and visit adjacent Os^{6+} sites to reach the opposite face. Differently colored spheres represent Ca^{2+} (blue) and doped Na^{+} (yellow) ions, and different osmium sites which are (i) surrounded by Ca^{2+} (red) or (ii) neighboring to a Na^{+} site (red highlighted with blue). Nodes have been numbered in the order in which they are visited, and we have applied PBCs. The algorithm has the following steps: (i) start at a vertex of the graph (ii) mark the current vertex as visited (iii) iterate through the adjacent vertices (iv) if an adjacent vertex has been visited, it is ignored (v) if an adjacent vertex has not been visited, recursively perform DFS on this vertex. The DFS algorithm explores a path as far as possible before backtracking and exploring other paths; for instance, the search pauses at the node-7, backtracks to node-6, and proceeds down a different branch via node-8.

Fig. 1(b). As we keep adding Na^{+} dopants, if we find a site where osmium magnetism is already suppressed, we assume that it remains suppressed. This leads to two types of sites at any concentration $\delta = (1-x)$ of Na^{+} dopants: those sites which are not neighbors of any dopant remain active in octupolar Ising magnetism, while a site which is a neighbor of any Na^{+} dopant effectively gets removed from the fcc lattice. We will use Monte Carlo simulations to realize various random configurations of Na^{+} for each x, and find the value of x at which the octupolar Os^{6+} ions stop percolating across the osmium fcc lattice.

A. Percolation threshold for correlated percolation

To determine the percolation threshold for this correlated percolation problem on the fcc lattice, we vary the probability of doping from $x = 1$ to $x = 0$ (equivalently Na^{+} concentration from $\delta = 0$ to $\delta = 1$) in increments of 0.01. We generate 20000 random instances for the dopant configuration at each value of x. For each instance, we use the Depth First Search (DFS) algorithm [35] to check

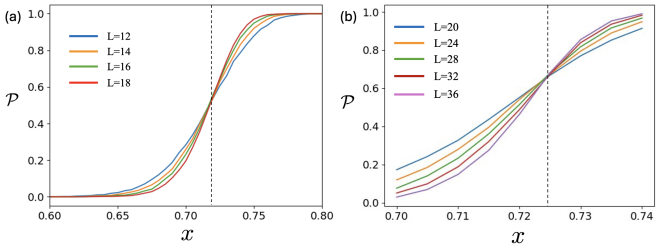

FIG. 3. Probability of percolation $\mathcal{P}$ as a function of x for linear system sizes (a) $L = 12, 14, 16, 18$ and larger sizes (b) $L = 20, 24, 28, 32, 36$. The intersection point of these graphs reveals the percolation threshold of $x_c \approx 0.717$ on smaller sizes and $x_c \approx 0.725$ on larger system sizes. Our best estimate using system sizes upto $L = 52$ yields $x_c = 0.7255(10)$.

whether the configuration of Os^{6+} ions percolates across the lattice, and thus compute the fraction $\mathcal{P}$ of all configurations which percolate. The DFS traversal order in a graph is shown in Fig. 2. DFS is appropriate for the percolation problem, as it efficiently traverses between pairs of opposite faces in the lattice. Fig. 3(a) and Fig. 3(b) show plots of $\mathcal{P}$ as a function of x for a set of system sizes L = 12-18 and larger sizes L = 20-36. We identify the intersection point of these various curves as the percolation threshold x_c. On smaller system sizes, we find $x_c \approx 0.717$, while on larger system sizes the threshold moves to $x_c \approx 0.725$. Going to larger system sizes upto $L = 52$, we determine $x_c = 0.7255(10)$ at which the probability $\mathcal{P}(x_c)$ becomes nearly system size independent corresponding to a crossing of the $\mathcal{P}(x)$ curves. This corresponds to a critical Na^{+} dopant concentration $\delta_c = 1 - x_c = 0.2745(10)$ beyond which connected Os^{6+} sites on the fcc lattice no longer percolate, so long-range octupolar Ising order can no longer exist.

We can contrast this with two other percolation thresholds we can estimate for uncorrelated percolation on the fcc lattice. If each dopant only knocks out a single Os^{6+} ion in its vicinity, the percolation problem reduces to the conventional site percolation model on the fcc lattice for which it is well known that $x_c \approx 0.1992$ [36–38]. This means a large doping concentration $\delta_c \approx 0.8008$ Na^{+} would be needed to kill octupolar magnetism. If, on the other hand, we assume each Na^{+} dopant removes six *randomly located* Os^{6+} ions on the fcc lattice, an admittedly artificial model, then $\delta_c \approx 0.1335$ so a much smaller doping would be needed to kill octupolar order than in our correlated percolation model.

B. Fractal dimension of percolation cluster

Consider the number $N_{\rm con}$ of Os^{6+} sites on the largest connected cluster. In the percolating phase, we expect $N_{\rm con} \sim L^3$, while in the non-percolating phase we expect $N_{\rm con} \sim L^0$. At the percolation threshold x_c, the size of the spanning cluster is expected to be a fractal, so the number of points on the cluster will scale as $N_{\rm con} \sim L^{d_f}$,

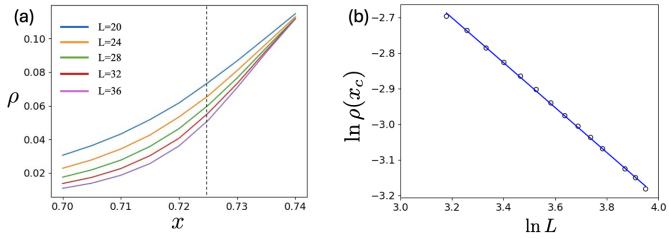

FIG. 4. (a) Cluster density ρ, defined as the largest connected cluster size $N_{\rm con}$ divided by total system volume L^3, plotted versus x; dashed line indicates the percolation threshold x_c. (b) Log-log plot of the cluster density at the percolation threshold $x_c = 0.7255$ versus the linear system size L for system sizes upto $L = 52$. From the slope of the linear fit we find the fractal dimension $d_f \approx 2.37$.

where d_f is the fractal dimension. Fig. 4(a) plots the system size dependence of the cluster density defined as $\rho = N_{\rm con}/L^3$, where we expect at criticality $\rho(x_c) \sim L^{d_f-3}$. To extract d_f, we plot $\ln \rho(x_c)$ versus $\ln L$ in Fig. 4(b), where we expect $\ln \rho(x_c) = (d_f - 3) \ln L +$ constant. A straight fit to the data on system sizes $L = 24, 28, \ldots, 52$ yields $d_f \approx 2.37$. Based on universality for percolation in the presence of short-range correlations, we might expect a larger $d_f \approx 2.52$ [36, 39–41]; it is possible that the universal value will be recovered if we work on much larger system sizes. At the same time, it is important to note that it has been suggested that the fractal dimension of the percolation cluster in certain models may be non-universal [42].

III. ISING MODEL ON PERCOLATING CLUSTERS

Finally, we turn to a study of the Ising model on the largest percolating cluster for $x_c < x \leq 1$. In the Ising model, spins are assigned values $s_i = \pm 1$ corresponding to the two octupolar states related by time-reversal symmetry. The Ising model Hamiltonian is given by

$$H = -J \sum_{\langle ij \rangle} s_i s_j \qquad (1)$$

where $J > 0$ is the interaction energy (octupolar exchange energy) which favors a state where all $\{s_i\} = +1$ or all $\{s_i\} = -1$. For Ba_2CaOsO_6, it has been estimated that $J \approx 1\,$meV [29], while quantum terms which could lead to dynamics are much weaker and can be ignored to leading approximation. The sites i, j are neighboring sites on the fcc lattice which form part of the connected percolating cluster and which have not been impacted by having a neighboring Na^+ dopant. To calculate the properties such as the Ising phase transition, we focus on only this percolating cluster of Os^{6+} spins, which can display a thermal phase transition to long-range magnetic order.

We begin by creating random disorder configurations of the dopants and identifying the largest connected cluster on the fcc lattice at each x. Using the Metropolis algorithm, we then perform Monte Carlo simulations of the Ising spin model on this connected cluster, fixing $J = 1$ which is equivalent to measuring temperature in units of J. At each temperature, we carry out simulations using a single spin flip Metropolis algorithm, where we consider a spin flip and calculate the resulting energy change ΔE. The flip is always accepted if it lowers the energy ($\Delta E < 0$) . If it increases the energy, the flip is accepted with probability $e^{-\Delta E/T}$ (we set $k_B = 1$). We use 10^4 sweeps of the percolating cluster to bring the spin configurations to thermal equilibrium, and study temperatures from $T = 15$ down to $T = 0.1$ in steps of 0.1. We then measure the energy over 10^5 sweeps of the percolating cluster, and use this to compute the specific heat per spin as a function of temperature. Finally, we average our results over 20 disorder realizations.

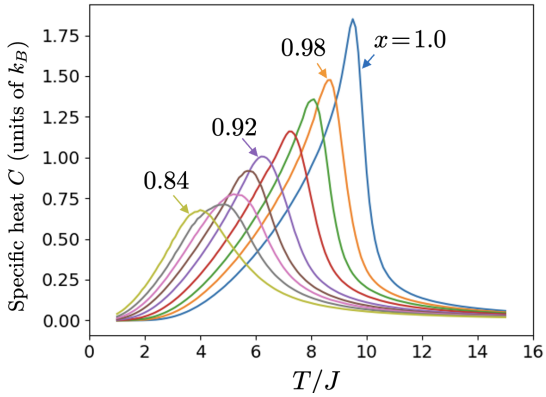

FIG. 5. Specific heat C per spin as a function of normalized temperature T/J for the Ising model on the largest percolating cluster for fixed lattice size $L = 12$ and varying concentrations $x = 1, 0.98, ..., 0.84$. The peak position of C yields the octupolar transition temperature T_c.

A. Specific Heat

To calculate the specific heat per spin, C, we use the the formula

$$C = \frac{\langle E^2 \rangle - \langle E \rangle^2}{N_c T^2} \qquad (2)$$

where E is the total energy, N_c is the number of spins in the cluster, and T is the temperature. The averages $\langle . \rangle$ correspond to Metropolis configuration averages for a fixed disorder realization. Fig. 5 shows C averaged over 20 disorder realizations plotted as a function of temperature, for different dopant concentrations which correspond to $x = 1.00, 0.98, \ldots 0.84$ in steps of 0.02. For $x = 1$, we find a peak in C from which we identify a phase transition into octupolar magnetic order at $T/J \approx 9.5$. With increasing x, we find that the peak in C moves to lower temperature, and the value of C also

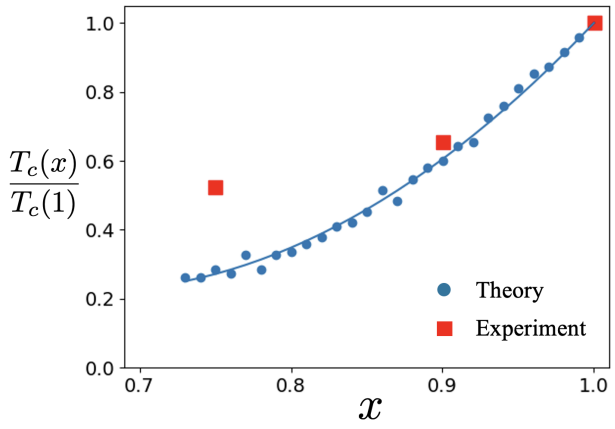

FIG. 6. Octupolar transition temperature $T_c(x)$ at various concentrations x scaled to its value at $x = 1$ (blue dots). Solid line is shown as a guide to the eye. We compare our results with T_c obtained using μSR experiments (red squares) as reported in Ref. [22].

decreases. We have checked, for consistency, that the integral $\int dT \frac{C}{T} \approx \ln 2$ over the shown temperature range for all values of x.

B. Octupolar transition temperature versus x

We finally turn to the octupolar transition temperature T_c which we identify using the peak position of the specific heat. Fig. 6 shows the Monte Carlo result for T_c as blue dots which we connect with a line as a guide to the eye. To permit a conparison of our results with experimental data, we normalize the value of T_c with its value in the clean system at $x = 1$. The normalized experimental data are shown as red squares in Fig. 6.

IV. CONCLUSION

In this paper, we proposed and studied a correlated percolation problem on the face-centred cubic lattice, and an Ising model on percolating clusters, in order to explain the octupolar magnetism of the doped double perovskite $Ba_2Na_{1-x}Ca_xOsO_6$. We computed the percolation threshold and fractal dimension using Monte Carlo simulations of the percolation model over a wide range of lattice sizes. Our critical temperature values from Monte Carlo simulations based on the Metropolis algorithm provide a good description of the experimental result for T_c for small Na doping, but this agreement breaks down for large Na doping at $x \leq 0.75$. This breakdown might possibly arise from the fact that we have retained the Os^{6+} sites in our model, but dropped $Os^{6+\varepsilon}$-Os^{6+} and $Os^{6+\varepsilon}$-$Os^{6+\varepsilon}$ interactions which might become more important at higher Na doping. Our work calls for additional experiments in the doping range $0.75 < x < 1$ to test for the range of validity of our model and when precisely it breaks down. Additional theoretical modelling is necessary to understand the magnetism of these disordered double perovskites $Ba_2Na_{1-x}Ca_xOsO_6$ for all dopings $0 < x < 1$.

ACKNOWLEDGMENTS

I thank Professor Arun Paramekanti for suggesting this problem, and for assistance with polishing the initial draft of this manuscript into a form suitable for journal submission.

Author contributions: The author wrote all the Python simulation codes, carried out all the simulations, and created the figures and plots for all the results presented in this paper.

Code availability: The Python Monte Carlo simulation codes for the percolation model and Ising model, as well as the codes and data for generating the figures in this paper are available on GitHub (https://github.com/Tanmay337442/percolationmagnet).

[1] J. Gopalakrishnan, A. Chattopadhyay, S. B. Ogale, T. Venkatesan, R. L. Greene, A. J. Millis, K. Ramesha, B. Hannoyer, and G. Marest, Metallic and nonmetallic double perovskites: A case study of A_2FeReO_6 (A = Ca, Sr, Ba), Phys. Rev. B **62**, 9538 (2000).

[2] W. Prellier, V. Smolyaninova, A. Biswas, C. Galley, R. L. Greene, K. Ramesha, and J. Gopalakrishnan, Properties of the ferrimagnetic double perovskites a2fereo6 (a = ba and ca), Journal of Physics: Condensed Matter **12**, 965 (2000).

[3] D. Sarma, A new class of magnetic materials: Sr2femoo6 and related compounds, Current Opinion in Solid State and Materials Science **5**, 261 (2001).

[4] D. Serrate, J. M. D. Teresa, and M. R. Ibarra, Double perovskites with ferromagnetism above room temperature, Journal of Physics: Condensed Matter **19**, 023201 (2006).

[5] H. Das, M. De Raychaudhury, and T. Saha-Dasgupta, Moderate to large magneto-optical signals in high Tc double perovskites, Applied Physics Letters **92**, 201912 (2008).

[6] T. Saha-Dasgupta, Magnetism in double perovskites, Journal of Superconductivity and Novel Magnetism **26**, 1991 (2013).

[7] S. Vasala and M. Karppinen, $A_2B'B''O_6$ perovskites: A review, Progress in Solid State Chemistry **43**, 1 (2015).

[8] A. E. Fedorovskiy, N. A. Drigo, and M. K. Nazeeruddin, The role of Goldschmidt's tolerance factor in the formation of A_2BX_6 double halide perovskites and its optimal range, Small Methods **4**, 1900426 (2020).

[9] H. A. Evans, L. Mao, R. Seshadri, and A. K. Cheetham, Layered double perovskites, Annual Review of Materials Research **51**, 351 (2021).

[10] A. Dey, J. Ye, A. De, E. Debroye, S. K. Ha, E. Bladt, A. S. Kshirsagar, Z. Wang, J. Yin, Y. Wang, L. N. Quan, F. Yan, M. Gao, X. Li, J. Shamsi, T. Debnath, M. Cao, M. A. Scheel, S. Kumar, J. A. Steele, M. Gerhard, L. Chouhan, K. Xu, X.-g. Wu, Y. Li, Y. Zhang, A. Dutta, C. Han, I. Vincon, A. L. Rogach, A. Nag, A. Samanta, B. A. Korgel, C.-J. Shih, D. R. Gamelin, D. H. Son, H. Zeng, H. Zhong, H. Sun, H. V. Demir, I. G. Scheblykin, I. Mora-Ser, J. K. Stolarczyk, J. Z. Zhang, J. Feldmann, J. Hofkens, J. M. Luther, J. Prez-Prieto, L. Li, L. Manna, M. I. Bodnarchuk, M. V. Kovalenko, M. B. J. Roeffaers, N. Pradhan, O. F. Mohammed, O. M. Bakr, P. Yang, P. Mller-Buschbaum, P. V. Kamat, Q. Bao, Q. Zhang, R. Krahne, R. E. Galian, S. D. Stranks, S. Bals, V. Biju, W. A. Tisdale, Y. Yan, R. L. Z. Hoye, and L. Polavarapu, State of the art and prospects for halide perovskite nanocrystals, ACS Nano **15**, 10775 (2021), pMID: 34137264.

[11] W.-J. Yin, J.-H. Yang, J. Kang, Y. Yan, and S.-H. Wei, Halide perovskite materials for solar cells: a theoretical review, J. Mater. Chem. A **3**, 8926 (2015).

[12] A. K. Jena, A. Kulkarni, and T. Miyasaka, Halide perovskite photovoltaics: Background, status, and future prospects, Chemical Reviews **119**, 3036 (2019).

[13] S. V. Streltsov and D. I. Khomskii, Jahn-Teller effect and spin-orbit coupling: Friends or foes?, Phys. Rev. X **10**, 031043 (2020).

[14] G. Khaliullin, D. Churchill, P. P. Stavropoulos, and H.-Y. Kee, Exchange interactions, Jahn-Teller coupling, and multipole orders in pseudospin one-half $5d^2$ Mott insulators, Phys. Rev. Research **3**, 033163 (2021).

[15] G. Chen, R. Pereira, and L. Balents, Exotic phases induced by strong spin-orbit coupling in ordered double perovskites, Phys. Rev. B **82**, 174440 (2010).

[16] G. Chen and L. Balents, Spin-orbit coupling in d^2 ordered double perovskites, Phys. Rev. B **84**, 094420 (2011).

[17] L. Lu, M. Song, W. Liu, A. P. Reyes, P. Kuhns, H. O. Lee, I. R. Fisher, and V. F. Mitrović, Magnetism and local symmetry breaking in a Mott insulator with strong spin orbit interactions, Nat. Comm. **8**, 14407 (2017).

[18] W. Liu, R. Cong, E. Garcia, A. Reyes, H. Lee, I. Fisher, and V. Mitrović, Phase diagram of Ba_2NaOsO_6, a Mott insulator with strong spin orbit interactions, Physica B: Condensed Matter **536**, 863 (2018).

[19] D. Hirai and Z. Hiroi, Successive symmetry breaking in a $j_{\rm eff} = 3/2$ quartet in the spin-orbit coupled insulator Ba_2MgReO_6, J. Phys. Soc. Jpn. **88**, 064712 (2019).

[20] D. Hirai, H. Sagayama, S. Gao, H. Ohsumi, G. Chen, T. Arima, and Z. Hiroi, Detection of multipolar orders in the spin-orbit-coupled $5d$ Mott insulator Ba_2MgReO_6, Phys. Rev. Research **2**, 022063 (2020).

[21] C. Svoboda, W. Zhang, M. Randeria, and N. Trivedi, Orbital order drives magnetic order in $5d^1$ and $5d^2$ double perovskite Mott insulators, Phys. Rev. B **104**, 024437 (2021).

[22] R. Cong, E. Garcia, P. C. Forino, A. Tassetti, G. Allodi, A. P. Reyes, P. M. Tran, P. M. Woodward, C. Franchini, S. Sanna, and V. F. Mitrović, Effects of charge doping on Mott insulator with strong spin-orbit coupling, $Ba_2Na_{1-x}Ca_xOsO_6$, Phys. Rev. Mater. **7**, 084409 (2023).

[23] J.-R. Soh, M. E. Merkel, L. Pourovskii, I. Zivkovic, O. Malanyuk, J. Pasztorova, S. Francoual, D. Hirai, A. Urru, D. Tolj, D. Fiore-Mosca, O. Yazyev, N. A. Spaldin, C. Ederer, and H. M. Ronnow, Spectroscopic signatures and origin of a hidden order in Ba_2MgReO_6 (2023), arXiv:2312.01767 [cond-mat.str-el].

[24] D. F. Mosca, C. Franchini, and L. V. Pourovskii, Interplay of superexchange and vibronic effects in the hidden order of Ba_2MgReO_6 unravelled from first principles (2024), arXiv:2402.15564 [cond-mat.str-el].

[25] D. D. Maharaj, G. Sala, M. B. Stone, E. Kermarrec, C. Ritter, F. Fauth, C. A. Marjerrison, J. E. Greedan, A. Paramekanti, and B. D. Gaulin, Octupolar versus néel order in cubic $5d^2$ double perovskites, Phys. Rev. Lett. **124**, 087206 (2020).

[26] A. Paramekanti, D. D. Maharaj, and B. D. Gaulin, Octupolar order in d-orbital Mott insulators, Phys. Rev. B **101**, 054439 (2020).

[27] S. Voleti, D. D. Maharaj, B. D. Gaulin, G. Luke, and A. Paramekanti, Multipolar magnetism in d-orbital systems: Crystal field levels, octupolar order, and orbital loop currents, Phys. Rev. B **101**, 155118 (2020).

[28] L. V. Pourovskii, D. F. Mosca, and C. Franchini, Ferro-octupolar order and low-energy excitations in d^2 double perovskites of osmium, Phys. Rev. Lett. **127**, 237201 (2021).

[29] S. Voleti, A. Haldar, and A. Paramekanti, Octupolar order and Ising quantum criticality tuned by strain and dimensionality: Application to d-orbital Mott insulators, Phys. Rev. B **104**, 174431 (2021).

[30] D. Churchill and H.-Y. Kee, Competing multipolar orders in a face-centered cubic lattice: Application to the osmium double perovskites, Phys. Rev. B **105**, 014438 (2022).

[31] S. W. Lovesey and D. D. Khalyavin, Lone octupole and bulk magnetism in Osmate $5d^2$ double perovskites, Phys. Rev. B **102**, 064407 (2020).

[32] S. W. Lovesey, D. D. Khalyavin, G. van der Laan, and G. J. Nilsen, Diffraction by multipoles in a $5d^2$ rhenium double perovskite, Phys. Rev. B **103**, 104429 (2021).

[33] S. Voleti, K. Pradhan, S. Bhattacharjee, T. Saha-Dasgupta, and A. Paramekanti, Probing octupolar hidden order via janus impurities, npj Quantum Materials **8**, 42 (2023).

[34] L. Celiberti, D. Fiore Mosca, G. Allodi, L. V. Pourovskii, A. Tassetti, P. C. Forino, R. Cong, E. Garcia, P. M. Tran, R. De Renzi, P. M. Woodward, V. F. Mitrović, S. Sanna, and C. Franchini, Spin-orbital jahn-teller bipolarons, Nature Communications **15**, 2429 (2024).

[35] J. Wengrow, *A Common-Sense Guide to Data Structures and Algorithms: Level Up Your Core Programming Skills*, edited by B. MacDonald (Pragmatic Bookshelf, 2020).

[36] X. Xu, J. Wang, J.-P. Lv, and Y. Deng, Simultaneous analysis of three-dimensional percolation models, Frontiers of Physics **9**, 113119 (2013).

[37] C. D. Lorenz and R. M. Ziff, Universality of the excess number of clusters and the crossing probability function in three-dimensional percolation, Journal of Physics A: Mathematical and General **31**, 81478157 (1998).

[38] K. Malarz, Simple cubic random-site percolation thresholds for neighborhoods containing fourth-nearest neigh-

bors, Physical Review E **91**, 10.1103/physreve.91.043301 (2015).

[39] Y. Deng and H. W. J. Blöte, Monte carlo study of the site-percolation model in two and three dimensions, Phys. Rev. E **72**, 016126 (2005).

[40] C. D. Lorenz and R. M. Ziff, Precise determination of the bond percolation thresholds and finite-size scaling corrections for the sc, fcc, and bcc lattices, Physical Review E **57**, 10.1103/physreve.57.230 (1998).

[41] H. G. Ballesteros, L. A. Fernndez, V. Martn-Mayor, A. M. Sudupe, G. Parisi, and J. J. Ruiz-Lorenzo, Scaling corrections: site percolation and ising model in three dimensions, Journal of Physics A: Mathematical and General **32**, 113 (1999).

[42] M. A. Knackstedt, M. Sahimi, and A. P. Sheppard, Nonuniversality of invasion percolation in two-dimensional systems, Phys. Rev. E **65**, 035101 (2002).